


Plasma wave oscillations in a nonequilibrium two-dimensional electron gas: Electric field induced plasmon instability in the terahertz frequency range

V. V. Korotyeyev ^{1,2} and V. A. Kochelap¹

¹*Department of Theoretical Physics, Institute of Semiconductor Physics of NAS of Ukraine, 03028, Kyiv, Ukraine*

²*Center for Physical Sciences and Technology, Saulėtekio al. 3, LT-10257, Vilnius, Lithuania*



(Received 13 April 2020; accepted 27 May 2020; published 9 June 2020)

We have developed a theory of collective electron oscillations in two-dimensional semiconductor heterostructures subjected to a high electric field. The effect of the stationary electric field has been taken into account on both steady-state and high-frequency electron transport. The analysis has been conducted by solving Boltzmann-Vlasov equations in the collisionless approach for high-frequency electron transport. Two actual types of heterostructures with *ungated* and *gated* two-dimensional (2D) electron gas have been considered. We have found that the collective excitation spectra of 2D electron gas are of the multibranch character with high-quality *plasmonic* modes and a set of *thermal* modes. Applied electric field induces the following effects: strong nonreciprocal behavior of both oscillation frequency and damping; interaction of plasmonic and thermal modes; instability of excitations propagating along the electron drift (effect of negative Landau damping). The mechanism of this plasma wave instability is different from early discussed Cherenkov, Dyakonov-Shur, and Ryzhii-Satou-Shur mechanisms of instabilities in plasmonic systems. It has been shown that the electrically induced plasmon instability provides amplification of terahertz (THz) radiation in grating-based plasmonic structures. We suggest that presented results can be important for deeper understanding of THz plasma physics and developing of electrically pumping devices for THz optoelectronics.

DOI: [10.1103/PhysRevB.101.235420](https://doi.org/10.1103/PhysRevB.101.235420)

I. INTRODUCTION

Collective plasma oscillations of electron gas in two-dimensional systems, i.e., 2D plasmons, are considerably different from conventional bulk three-dimensional (3D) plasmons. The 2D plasmons are realized in filmlike samples when scale of electron gas confinement w is much smaller than the wavelength λ of the plasmons propagating along the filmlike sample. The fundamental properties of 2D plasmons were investigated for different 2D systems including semiconductor quantum wells (QWs) [1–3], doped graphene [4,5], and other 2D crystals [6]. These studies revealed essential wave-vector dispersion of 2D-plasmon oscillations and their strong dependence on dielectric surrounding of two-dimensional electron gas (2DEG). For example, free-standing 2DEG exhibits a square-root wave-vector dependence of the plasmon frequency $\omega \sim \sqrt{q}$ (*ungated* plasmons), which becomes a linear dependence $\omega \sim q$ when metallic mirror is placed at the vicinity of 2DEG (*gated* plasmons).

Due to large mismatch of the wave vectors of electromagnetic waves and plasma waves of relevant frequency, their direct interaction is forbidden. To provide an effective coupling between the 2D plasmons and the electromagnetic waves, the 2DEG channel should be supplemented by a lateral structuring of the sample, for example, in the form of sub-wavelength metallic grating. Currently, such *hybrid plasmonic structures* are in the focus of interest of novel area of terahertz (THz) technologies, which is often called as THz plasmonics [7]. This research area is oriented to the development of compact solid-state devices with electrical pumping and

performance tuning, which is capable to modulate, detect, and emit/generate the electromagnetic waves of the THz frequency range. Indeed, the hybrid plasmonic structures with micron/nanoscale periods of the grating coupler possess the resonant properties in the THz frequency range.

The 2D-plasmon resonances were experimentally observed as a resonant absorption of the THz electromagnetic waves in different hybrid plasmonic structures based on Si inversion layer [8], GaAs/AlGaAs [9], AlGaIn/GaN [10,11] high-mobility heterostructures, doped graphene sheets [12,13], etc. These studies open the possibility to control the characteristic frequencies by the applied gate voltage [2,10,14] or lateral electric fields [15]. In the former case, the hybrid plasmonic structure with 2DEG can be configured as a grating-gate field-effect transistor (FET), where the plasmon spectra can be modified by an applied gate-to-channel voltage due to a spatial modulation of the 2DEG concentration. In the latter case, the applied lateral electric field renormalizes the plasmon spectra due to plasmonic nonreciprocity induced by the electron drift. This effect can be observed as a specific splitting of the frequency band of the plasmon resonance [16–18] and was measured by means of Raman spectroscopy [15] and the THz time-domain transmission/reflection spectroscopy [19].

The electrical control of the resonant properties of the hybrid plasmonic structures, as well as field induced plasmonic nonlinearity [16,20,21], were utilized for modulation [14,22] and detection [23,24] of the THz radiation. Meanwhile, the development of electrically driven plasmonic coherent THz sources still remains the great challenge for the modern THz technologies. The present achievements in this area are mainly

associated with selective THz emission [11,25,26] originated from the radiative decay of 2D plasmons of nonequilibrium 2DEG under the grating (see also Refs. [27,28]). Amplifying and generation of the THz radiation require the use of the effects of electrically induced plasmon instabilities.

In literature, different mechanisms of such instabilities are discussed. These include (i) Dyakonov-Shur instabilities in FETs [29,30] and diodes [31] with specific properties of the source and drain of the devices; (ii) Ryzhii-Satou-Shur transit-time instability which arises for the ballistic [32–34] or quasiballistic [35] electron transport; (iii) Cherenkov-type plasmon instability [18,36]. The latter can occur in grating-based plasmonic structures at the electron drift and can lead to appearance of a frequency band with negative absorption of the incident THz radiation. Another mechanism of electrically driven plasmon instability was proposed in Ref. [37] and is related to a strong renormalization of the plasmon spectra under the grating. This mechanism can be classified as an internal type of plasmon instabilities for a specific range of the wave vectors, for which the traveling plasmons are unstable. It can be mentioned also high-frequency Cherenkov-type instability in drifting plasmon-optical phonons system, that may arise in the reststrahlen frequency band [38–42].

The most mentioned theories and models are based on hydrodynamic treatment of the electron transport in the frame of the Euler-Poisson equation approach. This approach, particularly, implies high-electron concentrations, when strong electron-electron scattering controls both steady-state and high-frequency electron kinetics. However, the electron drift-induced instabilities critically require the use of high-mobility and low-doped plasmonic structures with deeply submicron grating periods to provide a decreasing of the plasmon damping and achieving the threshold velocity of the instability effects.

In fact, to observe and exploit the plasmon oscillations more favorable is the situation when the characteristic lateral scales of the plasmon excitations are shorter than the mean-free path of the electrons $ql_{sc} \gg 1$, and the frequencies are larger than the inverse scattering time $\omega\tau_{sc} \gg 1$. Then, the proper description of the collective electron excitations should be based on the more general *kinetic approach*, which uses the Boltzmann-Vlasov system of equations. Such theory for the collisionless bulk electron plasma *under equilibrium* has been developed many years ago by Landau [43,44] and later for 2D-electron plasma by Totsuji [45].

For nonequilibrium conditions, the impact of the electric field is typically taken into account by using the so-called shifted Maxwellian distribution, which ignores the effect of the electric field on electron high-frequency dynamics. The model of the nonequilibrium bulk plasma, which takes this effect into account, has been proposed and analyzed in the lowest order with respect to the electric field in the pioneer paper [46]. Authors have shown that applied electric field can decrease a damping of the plasmon mode propagating along the electron drift and even make this mode unstable. Later, for the same transport model, the high-frequency screening effect [47] and the two-stream instability [48] have been discussed.

Advances of modern technologies of semiconductor materials and devices, progress in instrumentations of the THz measurements, and increasing demands in THz

optoelectronic systems inspire serious interest to deeper analysis and understanding of the plasmonic properties. Recently, in the framework of the kinetic approach it was developed the theory of dynamic conductivity of graphene strips [49] and 2DEG in QWs [50]. These papers predicted the effect of the negative absorptivity in grating-based structures. The numerical simulation of the high-frequency electron transport in low-doped sheets of graphene [51] also confirmed the possibility of the plasmon instability induced by applied electric field.

In spite of number investigations, the detail analysis of collective excitation spectra for 2DEG subjected to a high electric field is absent in literature. In this paper, we present such an analysis for the case of two-dimensional electrons with the parabolic energy dispersion. The study of the high-frequency excitations of the electrons in the applied steady-state electric field E_0 is performed in the framework of general Landau approach, which is formulated as *initial value problem* for the Boltzmann-Vlasov system of equations assuming the collisionless approximation for the high-frequency electron dynamics. The characteristic equation for determination of the excitation spectra is formulated for arbitrary form of the steady-state distribution function and explicitly includes electric field effects on the high-frequency electron transport. The detail analysis of the excitations is performed with the use of the shifted Maxwellian steady-state distribution function. Two actual cases of the ungated and gated 2DEG are considered.

We found that the spectra of the collective oscillations of 2DEG have a multibranch character with two distinguished types of the excitations: *plasmonic* modes and *thermal* modes [52]. The plasmonic modes are high-quality oscillations with $\omega' \gg \omega''$, where ω' and ω'' are oscillation frequency and damping, respectively. In collisionless plasma, the imaginary part of the frequency ω'' arises due to the Landau damping mechanisms. The plasmonic modes are strongly influenced by the dielectric surroundings of the 2DEG. We showed that the Landau damping effect can be larger for the gated 2DEG in comparison to the ungated one. Under equilibrium, the thermal modes are the overdamped oscillations, with almost linear dispersion proportional to the thermal velocity of 2DEG.

At the presence of the electric field E_0 , the critical parameter responsible for renormalization of the mode damping is the relative gain of electron energy from the field E_0 on a distance of the order of the spatial period of the excitation wave $\gamma_q = eE_0/qk_B T_e$, where T_e is the electron temperature. We showed that this parameter controls the range of the wave vectors q where the negative Landau damping occurs, i.e., $\omega''(q) > 0$. Both types of the electron excitations can be unstable. We established that there are specific ranges of q and E_0 , where the plasmonic and thermal modes strongly interact.

The paper is organized as follows. The transport model, the basic system of equations, and the solution of the initial value problem are given in Sec. II. The characteristic equations for the electron excitations are analyzed in Sec. III. The derivation of plasmon spectra under equilibrium and nonequilibrium conditions for both the ungated and gated 2DEG are presented in Secs. IV and V, respectively. The obtained results are used for calculations of the absorption spectra of the particular

plasmonic AlGaAs/GaAs structure, Sec. VI. Conclusions are summarized in Sec. VII.

II. TRANSPORT MODEL AND BASIC EQUATIONS

The investigation of the high-frequency properties of the 2DEG is based on the system of equations which includes the Boltzmann transport equation (BTE)

$$\frac{\partial G}{\partial t} + \frac{\mathbf{p}}{m^*} \frac{\partial G}{\partial \mathbf{r}} + e \frac{\partial \Phi}{\partial \mathbf{r}} \bigg|_{z=0} \frac{\partial G}{\partial \mathbf{p}} = \hat{I}\{G\}, \quad (1)$$

the Poisson equation

$$\frac{\partial}{\partial \mathbf{r}} \left(\epsilon(z) \frac{\partial \Phi}{\partial \mathbf{r}} \right) + \frac{\partial}{\partial z} \left(\epsilon(z) \frac{\partial \Phi}{\partial z} \right) = 4\pi e [n(\mathbf{r}, t) - n_0] \delta[z], \quad (2)$$

and the following relationship between the electron concentration $n(\mathbf{r}, t)$ and the total electron distribution function $G(\mathbf{p}, \mathbf{r}, t)$:

$$n(\mathbf{r}, t) = \int_{-\infty}^{\infty} G(\mathbf{p}, \mathbf{r}, t) d\mathbf{p}. \quad (3)$$

The BTE is written for the parabolic and isotropic electron dispersion with a scalar effective mass m^* . The distribution function G depends on the electron momentum $\mathbf{p} = \{p_x, p_y\}$, the electron coordinate vector $\mathbf{r} = \{x, y\}$ (both are two-dimensional vectors) and the time t , $\hat{I}\{G\}$ is a collision integral. Then, $\Phi(\mathbf{r}, z, t)$ is the self-consistent electrostatic potential, n_0 is the equilibrium electron concentration of 2DEG, $\epsilon(z)$ describes dielectric surrounding of 2DEG, and $\delta[z]$ stands for the Dirac delta function.

Let a steady-state, uniform, and lateral electric field \mathbf{E}_0 be applied to 2DEG. This field induces a steady-state electron drift. The collective electron oscillations of the drifting 2DEG can be treated as small perturbations which are of a wavelike form. Under this assumption, the system of Eqs. (1)–(3) can be linearized. We present the function G as a sum of steady-state and high-frequency parts $G(\mathbf{p}, \mathbf{r}, t) = g_0(\mathbf{p}) + \tilde{g}_q(\mathbf{p}, t) \exp(i\mathbf{q}\mathbf{r})$, and the self-consistent potential as $\Phi(\mathbf{r}, z, t) = \tilde{\Phi}_q(z, t) \exp(i\mathbf{q}\mathbf{r})$, where \mathbf{q} is the wave vector of the wavelike perturbation. Now, Eqs. (1)–(3) can be written as follows:

$$-e\mathbf{E}_0 \frac{\partial g_0}{\partial \mathbf{p}} = \hat{I}\{g_0\}, \quad (4)$$

$$\frac{\partial \tilde{g}_q}{\partial t} + \frac{i\mathbf{q}\mathbf{p}}{m^*} \tilde{g}_q - e\mathbf{E}_0 \frac{\partial \tilde{g}_q}{\partial \mathbf{p}} = -ie\mathbf{q} \frac{\partial g_0}{\partial \mathbf{p}} \tilde{\Phi}_q(0, t), \quad (5)$$

$$\frac{\partial}{\partial z} \left(\epsilon(z) \frac{\partial \tilde{\Phi}_q}{\partial z} \right) - \epsilon(z) q^2 \tilde{\Phi}_q = 4\pi e \delta[z] \int_{-\infty}^{\infty} \tilde{g}_q(\mathbf{p}, t) d\mathbf{p}. \quad (6)$$

The function $g_0(\mathbf{p})$ is a solution of Eq. (4), in which all actual collision processes should be taken into account. Examples of calculations of such functions can be found elsewhere. The BTE for high-frequency perturbation, Eq. (5), is written in collisionless approximation. Applicability of this approximation will be estimated below for the particular cases. In what follows, we assume that $\mathbf{E}_0 = \{-E_0, 0\}$ and $\mathbf{q} = \{q, 0\}$, i.e., the electron gas drifts along the x axis in positive direction. Positive (negative) values of q correspond to the perturbations propagating along (opposite) the electron drift.

The Poisson equation (6) can be solved assuming appropriate boundary conditions. As a result, the high-frequency potential in the plane of 2DEG, $\tilde{\Phi}_q(0, t)$, reads as

$$\tilde{\Phi}_q(0, t) = -\frac{2\pi e}{|q|\kappa(|q|)} \int_{-\infty}^{\infty} \tilde{g}_q(\mathbf{p}, t) d\mathbf{p}, \quad (7)$$

where $\kappa(|q|)$ has a meaning of an effective dielectric permittivity. The explicit forms of $\kappa(|q|)$ for the gated and ungated heterostructures are given below [see Eq. (31)].

Following the Landau approach [43], we solve the initial value problem by using the direct and inverse Laplace transformations

$$\begin{bmatrix} \tilde{g}_{\omega, q}(\mathbf{p}) \\ \tilde{\Phi}_{\omega, q}(0) \end{bmatrix} = \int_0^{\infty} \begin{bmatrix} \tilde{g}_q(\mathbf{p}, t) \\ \tilde{\Phi}_q(0, t) \end{bmatrix} \exp(i\omega t) dt, \quad (8)$$

$$\begin{bmatrix} \tilde{g}_q(\mathbf{p}, t) \\ \tilde{\Phi}_q(0, t) \end{bmatrix} = \frac{1}{2\pi} \int_{-\infty+iis}^{\infty+iis} \begin{bmatrix} \tilde{g}_{\omega, q}(\mathbf{p}) \\ \tilde{\Phi}_{\omega, q}(0) \end{bmatrix} \exp(-i\omega t) d\omega. \quad (9)$$

Here, it is assumed $s > 0$, i.e., the complex variable $\omega = \omega' + i\omega''$ belongs to the upper half of the ω plane ($\omega'' > 0$). Using Eqs. (5) and (7) we obtain for the Laplace components

$$\tilde{g}_{iq} + i \left(\omega - \frac{qp_x}{m^*} \right) \tilde{g}_{\omega, q} - eE_0 \frac{\partial \tilde{g}_{\omega, q}}{\partial p_x} = ieq \frac{\partial g_0}{\partial p_x} \tilde{\Phi}_{\omega, q}(0), \quad (10)$$

$$\tilde{\Phi}_{\omega, q}(0) = -\frac{2\pi e}{|q|\kappa(|q|)} \int_{-\infty}^{\infty} \tilde{g}_{\omega, q}(\mathbf{p}) d\mathbf{p}, \quad (11)$$

with $\tilde{g}_{iq}(\mathbf{p})$ being a given initial perturbation of the electron distribution function in the moment $t = 0$. This function determines the initial perturbation of the electron concentration $\tilde{n}_{iq}(0) = \int \tilde{g}_{iq}(\mathbf{p}) d\mathbf{p}$, as well as the electrostatic potential $\tilde{\Phi}_q(0, 0) \equiv \tilde{\Phi}_i(0) = -2\pi e \tilde{n}_{iq}(0) / |q|\kappa(|q|)$. Solving Eq. (10), we find the Laplace components of the high-frequency part of distribution function:

$$\begin{aligned} \tilde{g}_{\omega, q}(\mathbf{p}) = & -\frac{iq\tilde{\Phi}_{\omega, q}(0)}{E_0} \int_{-\infty}^{p_x} dp'_x \frac{\partial g_0(p'_x, p_y)}{\partial p'_x} K_{\omega, q}(p_x, p'_x) \\ & + \frac{1}{eE_0} \int_{-\infty}^{p_x} dp'_x \tilde{g}_{iq}(p'_x, p_y) K_{\omega, q}(p_x, p'_x), \end{aligned} \quad (12)$$

where

$$K_{\omega, q}(p_x, p'_x) = \exp \left[\frac{i \{ \omega(p_x - p'_x) - q(p_x^2 - p_x'^2) / 2m^* \}}{eE_0} \right].$$

It should be noted that for ω defined in the upper half-plane, the Laplace component of the distribution function (12) tends to zero at $p_x \rightarrow \pm\infty$. Substituting Eq. (12) into Eq. (11) and using inverse Laplace transform (9) we can obtain temporal evolution of characteristics of 2DEG and the potential, which have a wavelike form with a given wave vector q . Particularly, for the self-consistent potential we have that

$$\tilde{\Phi}_q(0, t) = \frac{1}{2\pi} \int_{-\infty+iis}^{\infty+iis} d\omega \frac{\mathcal{N}(\omega, q)}{\Delta(\omega, q)} \exp(-i\omega t), \quad (13)$$

where the value of s should provide the way of integration above all poles of the function $\Delta(\omega, q)$. Functions $\mathcal{N}(\omega, q)$ and $\Delta(\omega, q)$ are given as follows:

$$\mathcal{N}(\omega, q) = \frac{\tilde{\Phi}_i(0)}{eE_0} \int_{-\infty}^{\infty} d\mathbf{p} \int_{-\infty}^{p_x} dp'_x \tilde{g}_{iq}(p'_x, p_y) \times K_{\omega, q}(p_x, p'_x), \quad (14)$$

$$\Delta(\omega, q) = 1 - \frac{2\pi i q e}{E_0 |q| \kappa(|q|)} \int_{-\infty}^{\infty} d\mathbf{p} \int_{-\infty}^{p_x} dp'_x \frac{\partial g_0(p'_x, p_y)}{\partial p'_x} \times K_{\omega, q}(p_x, p'_x). \quad (15)$$

These expressions can be simplified by reducing to single-integral forms:

$$\begin{aligned} \mathcal{N}(\omega, q) &= \tilde{\Phi}_i(0) \sqrt{\frac{-i\pi m^*}{2eE_0 q}} \int_{-\infty}^{\infty} dp_x \tilde{g}_i(p_x) \\ &\times \mathcal{W}_F \left[i \sqrt{\frac{iq}{2m^* e E_0}} \left(p_x - \frac{m^* \omega}{q} \right) \right], \quad (16) \\ \Delta(\omega, q) &= 1 - \frac{2\pi i q e n_0}{E_0 |q| \kappa(|q|)} \left\{ 1 - \sqrt{\frac{i\pi q}{2m^* e E_0}} \int_{-\infty}^{\infty} dp_x \tilde{g}_0(p_x) \right. \\ &\times \left. \left(p_x - \frac{m^* \omega}{q} \right) \mathcal{W}_F \left[i \sqrt{\frac{iq}{2m^* e E_0}} \left(p_x - \frac{m^* \omega}{q} \right) \right] \right\}. \quad (17) \end{aligned}$$

Here, $\tilde{g}_0(p_x) = \int dp_y g_0(p_x, p_y) / \int dp_x dp_y g_0(p_x, p_y)$ and $\tilde{g}_i(p_x) = \int dp_y \tilde{g}_{iq}(p_x, p_y) / \int dp_x dp_y \tilde{g}_{iq}(p_x, p_y)$ are the normalized electron distributions dependent on the only momentum p_x . Equations (16) and (17) can be applied for arbitrary forms of the functions g_0 and \tilde{g}_{iq} with a rapid (e.g., exponential) decrease at large momenta.

The integrals (16) and (17) contain the transcendental Faddeeva function $\mathcal{W}_F[\xi]$ [53], which is known for an arbitrary complex argument ξ . This provides the analytical continuation of $\mathcal{N}(\omega, q)$ and $\Delta(\omega, q)$ to the lower half of the complex ω plane, and facilitates estimates of the inverse Laplace transform (13). Indeed, the asymptotes of the integral in Eq. (13) at large t are determined by zeros of the function $\Delta(\omega, q)$, i.e., $\Phi_q(0, t) \sim \sum_k A_k \exp(-i\omega_k t)$, where ω_k are solutions of the *characteristic equation*

$$\Delta(\omega_k, q) = 0. \quad (18)$$

Thus, the temporal evolution of the high-frequency potential $\Phi_q(0, t)$ is defined by a superposition of different excitation modes oscillating with the frequencies ω_k . The amplitudes of these modes increase or decrease in time depending on signs of ω_k'' . Note, $\Delta(\omega, q)$ has the meaning of the dielectric response function of 2D plasma (see Refs. [44,45]).

III. CHARACTERISTIC EQUATION

The detail analysis of the collective excitation spectra $\omega_k(q)$ (k numerates possible different modes/branches), we perform for the so-called shifted Maxwellian distribution

function

$$g_0 = \frac{n_0}{2\pi m^* k_B T_e} \exp \left[-\frac{(p_x - m^* V_{dr})^2 + p_y^2}{2m^* k_B T_e} \right], \quad (19)$$

where V_{dr} and T_e are the drift velocity and electron temperature, respectively, and k_B is the Boltzmann constant. Two parameters V_{dr} and T_e are functions of the applied field E_0 . They can be found from Eq. (4) using the momentum and energy balance equations (see, for example, Refs. [54,55]).

For the distribution function (19), the main properties of the excitation spectra, including the effect of the high electric field, can be studied analytically. Indeed, the expression standing in the curly brackets of Eq. (17), denoted below as $I(\omega, q, E_0)$, can be presented in terms of function \mathcal{W}_F as follows:

$$I(\omega, q, E_0) = \frac{i\gamma_q}{1 + i\gamma_q} [1 + i\sqrt{\pi}\xi \mathcal{W}_F[\xi]], \quad (20)$$

$$\xi = \frac{\omega - V_{dr}q}{V_T |q| \sqrt{1 + i\gamma_q}}, \quad \gamma_q = \frac{eE_0}{qk_B T_e}, \quad V_T = \sqrt{\frac{2k_B T_e}{m^*}}. \quad (21)$$

Here, V_T is the thermal velocity of the electrons, the dimensionless complex variable $\xi = \xi' + i\xi''$ includes the critical parameter γ_q discussed in the Introduction. Then, the characteristic equation (18) takes the form

$$1 + \frac{q_D}{|q| \kappa(|q|)} \frac{1}{1 + i\gamma_q} [1 + i\sqrt{\pi}\xi \mathcal{W}_F[\xi]] = 0, \quad (22)$$

where $q_D = 2\pi e^2 n_0 / k_B T_e$ is the Debye wave number of non-degenerate 2DEG. Finally, Eq. (22) can be rewritten in the more compact form

$$Z(\xi) + Q + i\mathcal{E} = 0, \quad Z(\xi) = 1 + i\sqrt{\pi}\xi \mathcal{W}_F(\xi), \quad (23)$$

$$Q = \frac{\kappa(|q|)|q|}{q_D}, \quad \mathcal{E} = \gamma_q Q = \text{sgn}(q) \frac{\kappa(|q|)eE_0}{k_B T_e q_D}.$$

Now, determination of the excitation spectra is reduced to solutions of two transcendental equations

$$\begin{cases} Z'(\xi', \xi'') + Q = 0, \\ Z''(\xi', \xi'') + \mathcal{E} = 0, \end{cases} \quad (24)$$

where parameter Q is always positive and parameter \mathcal{E} can take both signs depending on the sign of q . The complex-valued function $Z(\xi) = Z'(\xi', \xi'') + iZ''(\xi', \xi'')$ is often mentioned as Jackson function [56]. This function has the following useful symmetry properties:

$$\begin{aligned} Z'(-\xi', \xi'') &= Z'(\xi', \xi''), \\ Z''(-\xi', \xi'') &= -Z''(\xi', \xi''). \end{aligned} \quad (25)$$

At the given Q and \mathcal{E} , the roots of the system (24) correspond to intersection points of two families of the curves in the $\{\xi', \xi''\}$ plane. These families are given by the first and second equations of the system (24). One of the family depends on the parameter Q , while the second one depends on the parameter \mathcal{E} . From the symmetry properties (25), it follows that roots of the system (24), obtained at positive \mathcal{E} ($q > 0$), including those belonging to the right and left half-spaces of the $\{\xi', \xi''\}$ plane, completely describe spectra of the electron oscillation.

Indeed, spectra of the modes propagating opposite electron drift ($q < 0$) can be easily obtained by means the substitutions

$$\xi' \rightarrow -\xi', \quad \xi'' \rightarrow \xi'', \quad q \rightarrow -q. \quad (26)$$

The solutions of Eqs. (24) allow us to find all possible roots ξ'_k and ξ''_k , where k will numerate the corresponding branches of the excitation spectra. Having these roots, we can restore [see the relationship in Eqs. (21)] the complex-valued frequency ω_k :

$$\omega_k = V_{dr}q + V_T|q|\sqrt{1 + i\gamma_q}\xi_k, \quad \xi_k = \xi'_k + i\xi''_k, \quad (27)$$

and obtain the oscillation frequency $\omega'_k(q)$ and decrement/increment $\omega''_k(q)$:

$$\begin{aligned} \omega'_k &= V_{dr}q + \frac{V_T|q|}{\sqrt{2}} \left[(\sqrt{1 + \gamma_q^2} + 1)^{\frac{1}{2}} \xi'_k \right. \\ &\quad \left. \mp (\sqrt{1 + \gamma_q^2} - 1)^{\frac{1}{2}} \xi''_k \right], \\ \omega''_k &= \frac{V_T|q|}{\sqrt{2}} \left[(\pm \sqrt{1 + \gamma_q^2} - 1)^{\frac{1}{2}} \xi'_k + (\sqrt{1 + \gamma_q^2} + 1)^{\frac{1}{2}} \xi''_k \right]. \end{aligned} \quad (28)$$

Here upper (lower) signs correspond to a positive (negative) γ_q .

The relationships (28) allow us to make the following important conclusions. (i) According to Eqs. (24) solutions ξ_k do not depend on V_{dr} . Thus, the only contribution from the drift velocity comes to the frequencies of the electron oscillations ω'_k by the Doppler-shift factor $V_{dr}q$. (ii) The decrements/increments of the excitations ω''_k are *independent* on V_{dr} . (iii) The electric field effect on the high-frequency electron dynamics, that corresponds to $\gamma_q \neq 0$, can lead to positive values of ω''_k , which means an instability of the excitation modes.

It is convenient to map the solutions on the $\{\xi', \xi''\}$ plane. As follows from the second equation of (28), there is a critical line in this plane defined as

$$\xi'' = -\frac{(\sqrt{1 + \gamma_q^2} - 1)^{\frac{1}{2}}}{(\sqrt{1 + \gamma_q^2} + 1)^{\frac{1}{2}}} \xi'. \quad (29)$$

The solutions of the system (24) calculated at $\gamma_q > 0$ and situated above the critical line correspond to the unstable modes ($\omega'' > 0$). Otherwise, the excitation modes are damped ($\omega'' < 0$).

IV. ELECTRON EXCITATION SPECTRA OF 2DEG UNDER EQUILIBRIUM ($\mathcal{E} = 0$)

As follows from Eqs. (28), under equilibrium the excitation spectra of 2DEG

$$\omega'_k = V_T|q|\xi'_k, \quad \omega''_k = V_T|q|\xi''_k, \quad (30)$$

are determined by the roots $[\xi'_k, \xi''_k]$ of the system (24) obtained at $\mathcal{E} = 0$. These roots depend on single dimensionless parameter Q , which has different physical meaning for the cases of the *ungated* (a) and *gated* (b) electron gas. In Figs. 1(a) and 1(b), the sketches of such systems are presented. There, the used below coordinate system, necessary

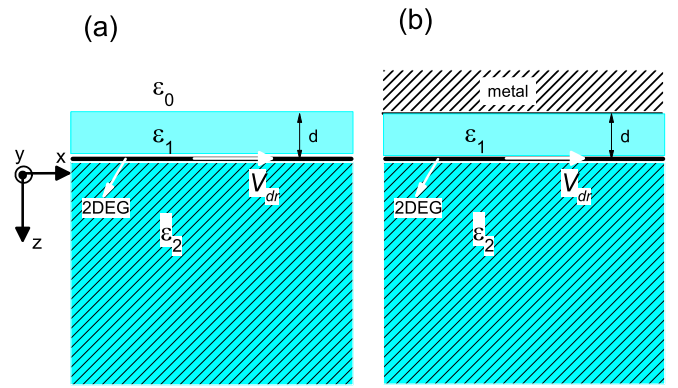


FIG. 1. Sketch of *ungated* (a) and *gated* by metallic mirror (b) heterostructures with 2DEG.

geometrical parameters, and characteristics of the dielectric environment are introduced.

Particularly, the effective dielectric permittivity $\kappa(|q|)$ introduced in Eq. (7) is expressed as follows (see for example Ref. [2]):

$$\kappa(|q|) = \begin{cases} \frac{1}{2} \left[\epsilon_2 + \epsilon_1 \frac{\epsilon_1 + \epsilon_0 \coth(|q|d)}{\epsilon_0 + \epsilon_1 \coth(|q|d)} \right] & \text{for (a),} \\ \frac{1}{2} [\epsilon_2 + \epsilon_1 \coth(|q|d)] & \text{for (b).} \end{cases} \quad (31)$$

In the limit of thin dielectric layer separating 2DEG from vacuum (a) or metal (b), i.e., $|q|d \ll 1$, we have $\kappa(|q|) = (\epsilon_0 + \epsilon_2)/2$ [for the structure (a)] and $\kappa(|q|) = \epsilon_1/2|q|d$ [for the structure (b)]. In this limit, we find the following expressions for Q :

$$Q = \begin{cases} \frac{\kappa|q|}{q_D} \equiv Q_{ng} & \text{(a),} \\ \frac{\epsilon_1}{2q_D d} = \frac{V_T^2}{2V_p^2} \equiv Q_g = \text{const} & \text{(b).} \end{cases} \quad (32)$$

Here,

$$V_p = \sqrt{\frac{4\pi e^2 n_0 d}{\epsilon_1 m^*}} \quad (33)$$

is the characteristic phase velocity of the gated 2D plasmons. In the case (a), Q is the module of the wave vector in units of the effective Debye wave number q_D/κ , where $\kappa = (\epsilon_0 + \epsilon_2)/2 = \text{const}$. In the case (b), Q does not depend on the wave vector.

A. Graphical analysis of the system (24) at $\mathcal{E} = 0$

The important peculiarities of the excitation spectra can be understood from mapping of solutions of the system (24) in the $\{\xi', \xi''\}$ plane, as presented in Fig. 2. At a given Q , the sought-for solutions are given by the intersection points of zero-level isolines of the functions $Z'(\xi', \xi'') + Q$ and $Z''(\xi', \xi'')$, respectively. As seen the presented isolines are of a multibranch character, which results in multiple solutions. In Fig. 2, these solutions are shown for two values of Q . As Q is varied, the solutions follow the *trajectories* indicated in Fig. 2. These trajectories coincide with segments of the zero-level isolines of the function $Z''(\xi', \xi'')$. The symmetrical

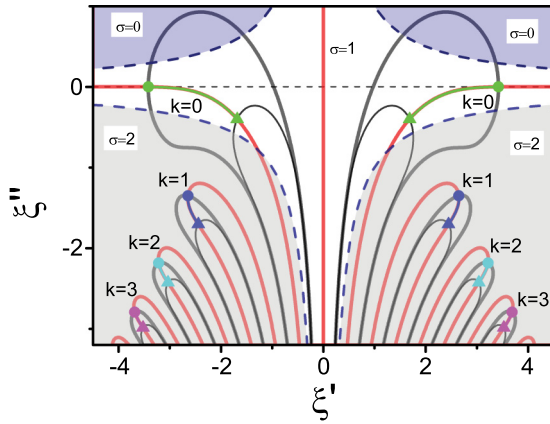


FIG. 2. Zero-level isolines of functions $Z''(\xi', \xi'')$ (red lines) and $Z'(\xi', \xi'') + Q$ (black lines). The latter calculated at $Q = 0.05$ (thick lines) and $Q = 0.5$ (thin lines). Colored curves with origins (marked by circles) and termini (marked by triangles) represent the trajectories of roots of Eqs. (24). Dashed lines represent the ratio $|\xi''| = 1/|\xi'|$ and demarcate regions, where parameter σ in Eq. (34) takes the values of 0, 1, and 2.

pairs of the trajectories at $\xi' > 0$ and $\xi' < 0$ correspond to two modes with the same oscillation frequency and damping, but propagating in the opposite directions. The location of the trajectories in the III and IV quadrants, where $\xi'' < 0$, points out the realization of only damped modes.

The two longest trajectories, which at small Q asymptotically are close to the $\xi'' = 0$ axis, correspond to the plasmonic modes ($k = 0$). These modes have highest quality factors $|\omega'/\omega''|$. Other modes with $k = 1, 2, \dots$ are described by much shorter trajectories and represent the overdamped oscillations. For them, $|\xi''| \sim |\xi'|$ and subsequently $|\omega'| \sim |\omega''|$. As shown below, these modes have practically linear dispersion and propagate with a velocity of the order of the thermal velocity V_T . We call them as the thermal modes. In general, increasing in Q leads to the progressive increasing of the $|\xi''|$ for all trajectories. The latter means that the Landau damping of all modes is increased with an increasing of Q .

B. Approximate formulas for excitation spectra and comparison with numerical results

The above analysis demonstrates that behavior of the roots of Eqs. (24) and, thus, oscillation frequencies, and dampings are very complicated. In order to understand better the excitation spectra, we can obtain asymptotic expressions for ξ'_k , ξ''_k and ω'_k , ω''_k . For that, we will use the following asymptotic expansions of the Jackson function $Z(\xi)$ [57]:

$$Z(\xi) = -1/2\xi^2 - 3/4\xi^4 - 15/8\xi^6 \dots + i\sigma\sqrt{\pi}\xi \exp(-\xi^2), \quad (34)$$

where $\sigma = 0$ if $\xi'' > |\xi'|^{-1}$, $\sigma = 1$ if $|\xi''| < |\xi'|^{-1}$ and $\sigma = 2$ if $\xi'' < -|\xi'|^{-1}$. That is, the asymptotes are different in different regions of the $\{\xi', \xi''\}$ plane. Five of such regions are marked in Fig. 2.

For the goal of this section we can omit the term $\propto 1/\xi^6$ in (34), then the characteristic equation (23) takes the form

$$-\frac{1}{2\xi^2} - \frac{3}{4\xi^4} - i\sigma\sqrt{\pi}\xi \exp(-\xi^2) + Q = 0. \quad (35)$$

At $Q \ll 1$, the plasmonic modes ($k = 0$) correspond to the roots with $|\xi''| < |\xi'|^{-1} \ll 1$, i.e., $\sigma = 1$. Then, approximate solutions of Eq. (35) are

$$\xi \approx \xi^{(0)} \left[1 + \frac{3}{4\xi^{(0)2}} - i\sqrt{\pi}\xi^{(0)3} \exp(-\xi^{(0)2}) \right], \quad (36)$$

with $\xi^{(0)} = \pm 1/\sqrt{2Q}$. Here, \pm correspond to the solutions situated in the left/right parts of the $\{\xi', \xi''\}$ plane, respectively. From Eq. (36), it follows that ξ'' has well-defined negative sign. As a result, both plasmonic modes have the same exponentially small damping at $Q \ll 1$. Using the relationships (30), we can recover the spectra of the plasmonic modes in the dimensional form

$$\begin{aligned} \omega'_0 &\approx \frac{V_T|q|}{\sqrt{2Q}} \left[1 + \frac{3Q}{2} \right], \\ \omega''_0 &\approx -\sqrt{\pi} \frac{V_T|q|}{\sqrt{2Q}} \left(\frac{1}{2Q} \right)^{3/2} \exp\left(-\frac{1}{2Q}\right). \end{aligned} \quad (37)$$

Now, for the ungated 2DEG when $Q = Q_{ng}$ [see Eqs. (32) (a)], we find

$$\begin{aligned} \omega'_0 &\approx \omega_p \left[1 + \frac{3\kappa|q|}{2q_D} \right], \\ \omega''_0 &\approx -\sqrt{\frac{\pi}{8}} \omega_p \left(\frac{q_D}{\kappa|q|} \right)^{3/2} \exp\left(-\frac{q_D}{2\kappa|q|}\right), \end{aligned} \quad (38)$$

where

$$\omega_p = \sqrt{\frac{2\pi e^2 n_0 |q|}{\kappa m^*}}$$

is the standard frequency of the ungated 2D plasmons [1].

For the gated 2DEG with $Q = Q_g$ [see definition in Eqs. (32)], we obtain

$$\begin{aligned} \omega'_0 &\approx V_p|q| \left[1 + \frac{3V_T^2}{4V_p^2} \right], \\ \omega''_0 &\approx -\sqrt{\pi} V_p|q| \frac{V_p^3}{V_T^3} \exp\left(-\frac{V_p^2}{V_T^2}\right), \end{aligned} \quad (39)$$

where V_p is defined by Eq. (33).

Comparison of Eqs. (38) and (39) shows that the Landau damping of the collisionless 2D plasma strongly depends on dielectric surrounding of 2DEG. For the ungated 2DEG, the damping of the plasmonic mode has the essential wave-vector dependence and is exponentially small at $\kappa|q|/q_D \ll 1$, similarly to the well-known case of 3D plasma. For the gated 2DEG, in the limit of $|q|d \ll 1$, the damping of the plasmonic mode has a linear dispersion and can be much larger than for the ungated one. However, Landau damping of the gated 2DEG can be also small if $V_p \gg V_T$.

Figure 2 shows us that another family of the solutions of Eqs. (24) with $k = 1, 2, \dots$, the thermal modes, is realized at $\xi'' < -|\xi'|^{-1}$ ($\sigma = 2$). By using the asymptotic series of

Eq. (34) we can obtain approximate expressions for these modes. At small Q , such that $Q \ll 1/4\pi k$, we find

$$\begin{aligned}\omega'_k &\approx V_T |q| x_k^{(0)} \left[1 + \frac{\ln[\sqrt{2\pi}(2x_k^{(0)})^3]}{4x_k^{(0)2}} + Q \dots \right], \\ \omega''_k &\approx -V_T |q| x_k^{(0)} \left[1 - \frac{\ln[\sqrt{2\pi}(2x_k^{(0)})^3]}{4x_k^{(0)2}} + Q \dots \right],\end{aligned}\quad (40)$$

where $x_k^{(0)} = \sqrt{\pi(k+1/8)}$ and $k = 1, 2, 3, \dots$. In these equations we omit terms $\propto 1/x_k^{(0)4}$. At the relatively larger Q , such that $Q \gg 1/4\pi k$, we obtain

$$\begin{aligned}\omega'_k &\approx V_T |q| x_k^{(0)} \left\{ 1 - \frac{1}{4x_k^{(0)2}} \ln \left[\frac{Q}{\sqrt{2\pi} 2x_k^{(0)}} \right] + \dots \right\}, \\ \omega''_k &\approx -V_T |q| x_k^{(0)} \left\{ 1 + \frac{1}{4x_k^{(0)2}} \ln \left[\frac{Q}{\sqrt{2\pi} 2x_k^{(0)}} \right] + \dots \right\},\end{aligned}\quad (41)$$

where $x_k^{(0)} = \sqrt{\pi(k+3/8)}$ and $k = 0, 1, 2, 3, \dots$. It should be noted that expressions (41) are also suitable for the asymptotic descriptions of the plasmonic modes ($k = 0$) at relatively large Q .

The obtained approximate formulas (40) and (41) indicate that the thermal modes have almost linear (for the ungated 2DEG) and strictly linear (for the gated 2DEG) dispersions of both $\omega'(q)$ and $\omega''(q)$ with the slopes, which are determined by the thermal velocity V_T . These modes are overdamped oscillations with $\omega' \sim |\omega''|$ and exhibit a weak dependence on the electron concentration and dielectric surrounding of 2DEG [see Eqs. (32)]. The high-order thermal modes have higher frequencies of oscillations and higher damping due to the prefactor $x_k^{(0)} \sim \sqrt{k}$. Moreover, they become less sensitive to the value of Q with increasing of k .

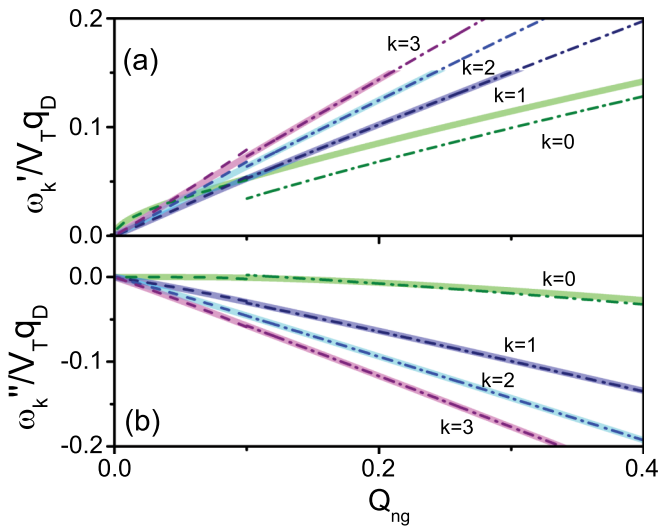


FIG. 3. Dependencies of $\omega'_k(q)$ (a) and $\omega''_k(q)$ (b) for the ungated 2DEG. The first four branches, $k = 0, 1, 2, 3$, are presented. Solid curves represent results of numerical calculations. Other curves are approximate expressions (38), (40) (dashed lines) and (41) (dashed-dotted lines).

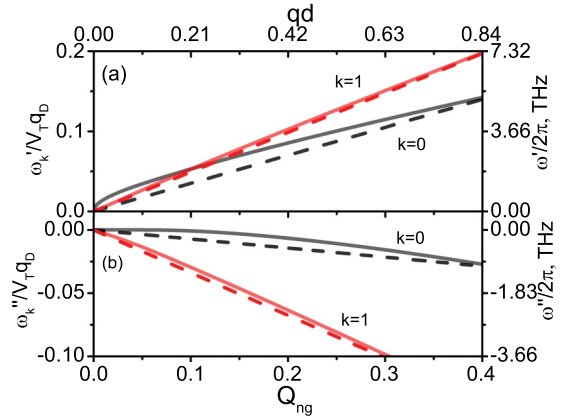


FIG. 4. Dependencies of $\omega'_k(q)$ (a) and $\omega''_k(q)$ (b). Solid and dashed lines are calculations for the ungated and gated 2DEG, respectively. Used parameters are listed in the text. Black and red lines correspond to the plasmonic and the first thermal modes, respectively.

Figure 3 illustrates the comparison between obtained approximate results and numerical calculations of the spectra of the ungated 2DEG. As seen, in the long-wavelength limit ($Q_{ng} \leq 0.1$), Eqs. (38) and (40) give the proper approximations for the plasmonic and thermal modes, respectively. At the $Q_{ng} \leq 0.1$ the plasmonic mode has negligibly small damping and square-root q dependence of the oscillation frequency. With increasing of q , the damping of the plasmonic modes increases. The square-root dependence of the oscillation frequency changes to a linear one according to (41). In the short-wavelength limit ($Q_{ng} \geq 0.1$), the spectra of both plasmonic and thermal modes are well described by Eqs. (41). The thermal modes in the considered range of q remain almost linear and overdamped. It should be noted that there are intersection points of dependencies $\omega'_0(q)$ and $\omega'_{1,2,\dots}(q)$. However, the plasmonic mode and the thermal modes do not interact because of a large difference of their damping. The latter can be also understood from Fig. 2, where, as seen, the trajectories of the roots for different modes are well separated.

C. Comparison of excitation spectra of the ungated and gated 2DEG

Comparison of the spectra of collective oscillations of the ungated and gated 2DEG is performed for the particular case of the AlGaAs/GaAs heterostructure with the following parameters: $n_0 = 1 \times 10^{11} \text{ cm}^{-2}$, $m^* = 0.063 \times m_e$ (m_e is the free-electron mass), and $T_e = 100 \text{ K}$. Dielectric permittivities of the barrier and buffer layers are assumed to be equal: $\epsilon_1 = \epsilon_2 = 9$. For the barrier layer of $d = 10 \text{ nm}$, the parameter describing the gated 2DEG is $Q_g = 0.42$. For the ungated 2DEG we find the effective dielectric permittivity $\kappa = 5$ and characteristic wave vector $q_D/\kappa = 2 \times 10^6 \text{ cm}^{-1}$.

For these parameters, the calculated spectra of the plasmonic and first thermal modes are shown in Fig. 4 for both ungated and gated 2DEG.

As seen, in the range of small wave vectors $Q_{ng} \leq 0.1$ the plasmonic mode for the ungated 2DEG exhibits square-root dependence of $\omega'(q)$ with negligibly small value of $\omega''(q)$. The same type of the mode for the gated 2DEG has lower frequencies and much greater damping. With increasing of wave vector, when Q_{ng} becomes ~ 0.3 , the plasmonic modes for both cases have comparable damping and oscillation frequencies. The thermal modes' spectra are less sensitive to the electrostatic surrounding of 2DEG. For example, the spectra of the first thermal modes for the both gated and ungated 2DEG practically coincide.

V. ELECTRON EXCITATION SPECTRA OF NONEQUILIBRIUM 2DEG ($\mathcal{E} \neq 0$)

A steady-state electric field E_0 applied to the 2DEG changes considerably the excitation spectra. The basic equations determining these spectra (24) and (28) are modified due to two factors dependent on the field. The first is the Doppler-shift term $V_{dr} q$ in Eqs. (28). As a result, the oscillation frequency $\omega'(q)$ acquires a nonreciprocal behavior along the field direction. The second factor is the gain/loss parameter $\gamma_q \neq 0$, which explicitly enters to Eqs. (28) that couples ω' , ω'' and the variables ξ' , ξ'' . In turn, ξ' , ξ'' are solutions of Eqs. (24) dependent on γ_q via the parameter \mathcal{E} . The latter parameter can be specified for the ungated (a) and gated (b) 2DEG as follows:

$$\mathcal{E} = \begin{cases} Q_{ng}\gamma_q = \frac{\text{sign}(q)\kappa e E_0}{k_B T_c q_D} = \frac{\text{sign}(q)\kappa E_0}{2\pi e n_0} \equiv \mathcal{E}_{ng} & \text{(a),} \\ Q_g\gamma_q = \frac{e E_0}{m^* V_p^2 q} \equiv \mathcal{E}_g & \text{(b).} \end{cases} \quad (42)$$

A. Graphical analysis of Eqs. (24) at $\mathcal{E} \neq 0$

We begin with the graphical analysis of Eqs. (24). We assume that $Q > 0$ and $\mathcal{E} > 0$, considering the entire $\{\xi', \xi''\}$ plane.

Figures 5 and 6 illustrate the mappings of the system (24) obtained at nonzero values of \mathcal{E} . The first equation of (24) does not contain the electric field, thus the corresponding zero-level isolines remain the same as in Fig. 2 for equilibrium. However, even a small value of \mathcal{E} , for example $\mathcal{E} = 0.015$, strongly deforms zero-level isolines of the function in the second equation in comparison to the equilibrium case. Now, the roots of the system (24) can belong to the quadrants II, III, and IV of the $\{\xi', \xi''\}$ plane. As seen, the trajectories of solutions corresponding to the plasmonic modes are located in the quadrants IV and II, predominantly. In the quadrant IV, it can occur a situation when the trajectories corresponding to the plasmonic mode and the thermal modes become very close. At this, a mode interaction effect is expected. Moreover, at least, the first four roots in quadrant IV obtained at small Q ($Q = 0.005$ corresponding to $\gamma_q = 3$) are situated above the critical line (line 1) defined by Eq. (29). It means that these modes have a negative damping, i.e., they are unstable. The other roots which belong to the quadrants II and III are located below the critical lines and they correspond to the damped oscillations.

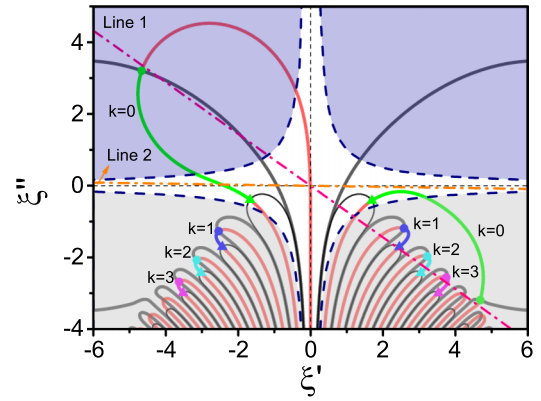


FIG. 5. Zero-level isolines of the functions $Z'(\xi', \xi'') + Q$ (black lines) and $Z''(\xi', \xi'') + \mathcal{E}$ (red lines) at $\mathcal{E} = 0.015$. Thick and thin black lines are for $Q = 0.005$ and 0.5 , respectively. Colored curves with origins (marked by circles) and termini (marked by triangles) are the trajectories of solutions obtained at variation of Q from 0.005 to 0.5 . Dashed-dotted lines 1 and 2 are the critical lines given by Eq. (29) for two values of γ_q : 3 and 0.03 .

At relatively large $Q = 0.5$ ($\gamma_q = 0.03$), all roots, including the quadrant IV, are situated below critical line (line 2). They correspond to the damped modes. We conclude that the modes corresponding to the roots from the quadrant IV, including the thermal modes, have a finite range of the wave vectors where they are unstable even at a small parameter \mathcal{E} .

With increase in \mathcal{E} the zero-level isolines of the function $Z''(\xi', \xi'') + \mathcal{E}$ are deformed in such way that trajectories of different solutions become well separated (see Fig. 6 for $\mathcal{E} = 0.15$). It means that the mode interaction effect is suppressed at higher electric fields. At this, the trajectory of the plasmonic solution becomes much shorter than those at smaller \mathcal{E} . A larger number of the thermal modes are unstable.

Below, we present asymptotic expressions of $\omega'_k(q)$ and $\omega''_k(q)$ for both structures presented in Fig. 1 subjected to the electric field.

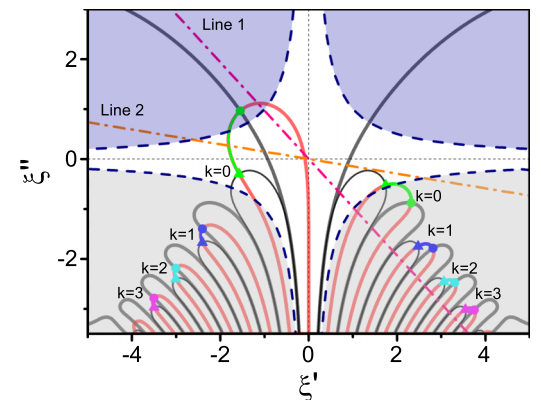


FIG. 6. The same as in Fig. 5 calculated at $\mathcal{E} = 0.15$.

B. Approximate formulas for excitation spectra at finite \mathcal{E}

Similarly to the procedure of calculations of approximate expressions for $\omega'_k(q)$ and $\omega''_k(q)$ presented in Sec. IV B, we will use the asymptotic series (34) keeping three terms in the power expansion. As seen from Fig. 5, the two longest trajectories for the plasmonic modes are mainly located in the region of the $\{\xi', \xi''\}$ plane where $|\xi'| > |\xi''| > 1$. The analytical solutions for corresponding roots of the system (24) can be found if $\xi'^2 - \xi''^2 \gg 1$. Thus, in the series (34) for the roots, which belong to the quadrants II and IV, we should set $\sigma = 0$ and 2, respectively.

As a result, we obtain the following approximate frequency and damping dependencies for the ungated 2DEG:

$$\begin{aligned} \omega'_0 &= V_{dr}q + \omega_p \left[1 + \frac{3\kappa|q|}{2q_D} + \frac{15}{8} \left(\frac{\kappa|q|}{q_D} \right)^2 (1 - \gamma_q^2) + \dots \right], \\ \omega''_0 &= \pm \frac{3}{2} \frac{eE_0}{m^*V_T} \sqrt{\frac{2\kappa|q|}{q_D}} \left[1 + \frac{5\kappa|q|}{2q_D} + \dots \right. \\ &\quad \left. \mp \frac{\sigma\sqrt{\pi}m^*V_T^2q_D}{3\kappa|q|eE_0} \exp\left(-\frac{q_D}{2\kappa|q|(1+\gamma_q^2)}\right) \right], \end{aligned} \quad (43)$$

and for the gated 2DEG

$$\begin{aligned} \omega'_0 &= V_{dr}q + V_p|q| \left[1 + \frac{3V_T^2}{4V_p^2} + \frac{15}{32} \frac{V_T^4}{V_p^4} (1 - \gamma_q^2) + \dots \right], \\ \omega''_0 &= \pm \frac{3}{2} \frac{eE_0}{m^*V_p} \left[1 + \frac{5V_T^2}{4V_p^2} + \dots \right. \\ &\quad \left. \mp \frac{2\sigma\sqrt{\pi}m^*V_p^2q}{3eE_0} \exp\left(-\frac{V_p^2}{V_T^2(1+\gamma_q^2)}\right) \right]. \end{aligned} \quad (44)$$

Here, “+” and $\sigma = 2$ correspond to the plasmon mode propagating along the electric field ($q > 0$ at $E_0 > 0$), while “−” and $\sigma = 0$ stand for the mode propagating in opposite direction ($q < 0$). Equations (43) and (44) are valid if

$$2Q(1 + \gamma_q^2) = 2(Q + \mathcal{E}^2/Q) \ll 1. \quad (45)$$

Note, at a given small \mathcal{E} the inequality (45) restricts the validity of Eqs. (43) and (44) by the interval $2\mathcal{E} < Q < \frac{1}{2}$. For example, for the plasmonic roots presented in Fig. 5 ($\mathcal{E} = 0.015$) the trajectories start at $Q = 0.005$, when the left-hand side of Eq. (45) is ≈ 0.1 , thus Eqs. (43) and (44) are applicable. The ends of these trajectories are at $Q = 0.5$ and the left-hand side of Eq. (45) is ≈ 1 , so the mentioned equations can not be used.

While the criterion (45) is fulfilled, Eqs. (43) and (44) indicate that the effect of the electric field is weak for $\omega'_0(q)$ in both ungated and gated 2DEG (except of the Doppler-shift term). However, the field strongly influences on $\omega''_0(q)$. Indeed, $\omega''_0(q)$ consists of two contributions. The first is a term linearly proportional to the field, the second is an exponentially small Landau-type damping, which is weakly dependent on the field. For the modes propagating along electron drift, the first term is positive. These modes can be unstable ($\omega''_0 > 0$), when the first term dominates over exponentially small

Landau-type damping. The field-dependent “increment” has square-root wave-vector dependence for the ungated 2DEG and almost independent on the wave vector for the gated 2DEG. The modes propagating in the direction opposite to the drift are always damped. In other words, the account of the electric field effect on high-frequency electron dynamics leads to nonreciprocal behavior of the plasmon damping. These effects are different from standard models of the instabilities in the drifting plasma [56,58].

The roots of Eqs. (24) for the *thermal* modes correspond to short trajectories in the $\{\xi', \xi''\}$ plane, as seen in Fig. 5. They are located in the quadrants IV and III. For them $|\xi'| \sim |\xi''| > 1$ and the exponential term in the expansion (34) can be of the same order with other power terms. We found approximate formulas for ω'_k , ω''_k with $k \geq 1$ for two limiting cases: $|\mathcal{E}| \ll |Q| \sim 1$ and $|Q| \ll |\mathcal{E}| \sim 1$. For $|\mathcal{E}| \ll |Q| \sim 1$ ($\gamma_q \ll 1$) the results practically coincide with Eqs. (41) with a small correction $\sim \gamma_q$.

In the case of $|Q| \ll |\mathcal{E}| \ll 1$ ($\gamma_q \gg 1$) we find the following asymptotic expressions:

$$\begin{aligned} \omega'_k|_{q>0} &\approx V_{dr}q + 2\sqrt{\frac{eE_0|q|}{m^*}} x_k^{(0)} \left[1 + \frac{x_k^{(1)}}{2\gamma_q x_k^{(0)}} + \dots \right], \\ \omega'_k|_{q<0} &\approx V_{dr}q + 2\sqrt{\frac{eE_0|q|}{m^*}} \left[x_k^{(1)} + \frac{x_k^{(0)}}{2\gamma_q} + \dots \right], \\ \omega''_k|_{q>0} &\approx 2\sqrt{\frac{eE_0|q|}{m^*}} \left[x_k^{(1)} - \frac{x_k^{(0)}}{2\gamma_q} + \dots \right], \\ \omega''_k|_{q<0} &\approx -2\sqrt{\frac{eE_0|q|}{m^*}} x_k^{(0)} \end{aligned} \quad (46)$$

with $x_k^{(0)} = \sqrt{\pi(k+1/8)}$ and $x_k^{(1)} = 1/4x_k^{(0)} \times \ln[\sqrt{2\pi}(2x_k^{(0)})^3/|1 \mp 4x_k^{(0)2}\mathcal{E}|]$ where \mp corresponds to $q > 0$ and $q < 0$, respectively. Application of these results is restricted by the condition $\mathcal{E} < 1/4\pi k$.

In the contrast to the plasmonic modes, the oscillation frequencies of the thermal modes are strongly renormalized even by a small electric field. From the results of Eqs. (46) it follows that the thermal modes propagating along electron drift $q > 0$ can be unstable, while the modes with $q < 0$ are damped.

When parameter \mathcal{E} is not small ($\mathcal{E} > 1/4\pi$), the trajectory of the roots of Eqs. (24) corresponding to the plasmonic mode in the quadrant IV acquires the form similar to the thermal modes, as seen from Fig. 6. This trajectory is located in the region where $\xi' \sim |\xi''|$. For this case and $\gamma_q \gg 1$ we found the asymptotic expressions for ω'_k and ω''_k in the form which coincides with Eqs. (46) for both the plasmonic and thermal modes. Now, in these equations one should set $x_k^{(0)} = \sqrt{\pi(k+5/8)}$ for $q > 0$ and $x_k^{(0)} = \sqrt{\pi(k+1/8)}$ for $q < 0$, and $x_k^{(1)} = -1/4x_k^{(0)} \times \ln[|\mathcal{E}|/\sqrt{2\pi}2x_k^{(0)}]$ for any sign of q ; $k = 0, 1, 2, \dots$

C. Results of numerical calculations

In this section we present numerical results for $\omega'_k(q)$ and $\omega''_k(q)$ at finite values of \mathcal{E} , as well as their comparison with the above-obtained asymptotic expressions.

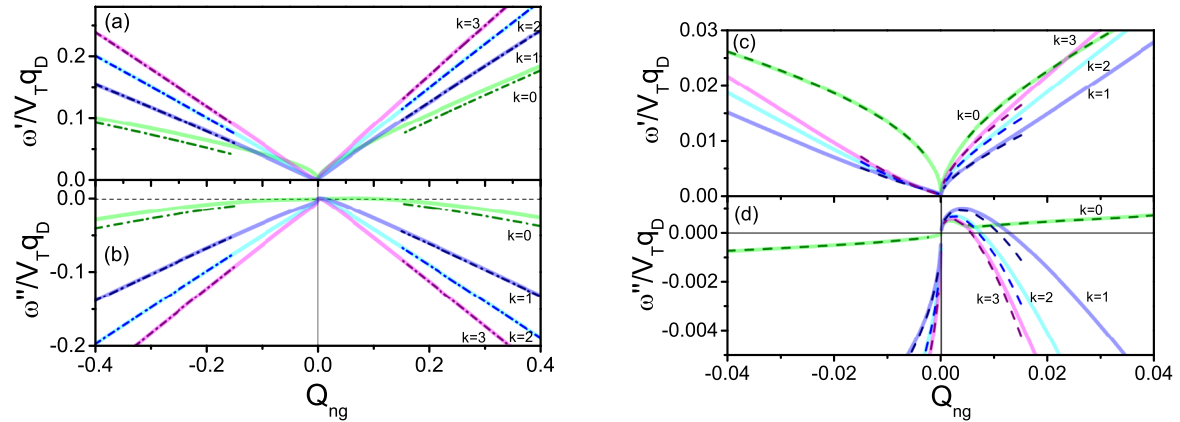


FIG. 7. Dependencies of $\omega'_k(q)$ (a) and $\omega''_k(q)$ (b) for ungated 2DEG at $\mathcal{E}_{ng} = 0.015$. Solid lines present the numerical calculations. Dashed-dotted lines are the asymptotes obtained in the limit of large Q_{ng} given by Eqs. (41). Panels (c) and (d) magnify the region of small Q_{ng} where dashed lines are the asymptotes given by Eqs. (43) for the $k = 0$ and Eqs. (46) for $k \neq 0$. Dimensionless drift velocity is $V_{dr}/V_T = 0.5$.

1. Ungated 2DEG

Figures 7 and 8 provide numerical results for four lowest modes at two values of \mathcal{E}_{ng} used in Figs. 5 and 6. The asymptotic expressions are also shown for comparison. At small $\mathcal{E}_{ng} = 0.015$, the plasmonic modes manifest themselves as high-quality oscillations with clear nonreciprocal behavior and small, but not exponentially small, value of $\omega''_0(q)$. At $q > 0$, a wide instability range of the wave vectors occurs, while the excitations with $q < 0$ are always damped. The asymptotic expressions for $\omega'_0(q)$, $\omega''_0(q)$ for the plasmonic modes of Eqs. (43) almost coincide with numerical results within the range of the dimensionless wave vectors $Q_{ng} = 0.01 \dots 0.05$, where the criterion (45) is well fulfilled.

At very small $Q_{ng} < 0.005$, the asymptotic expressions (43) are not valid, the numerical results for small q are presented in Figs. 7(c) and 7(d). One can see that for the analyzed modes the dampings $\omega''_k(q)$ are nonmonotonic functions. Apparently, there is an effect of interaction between the

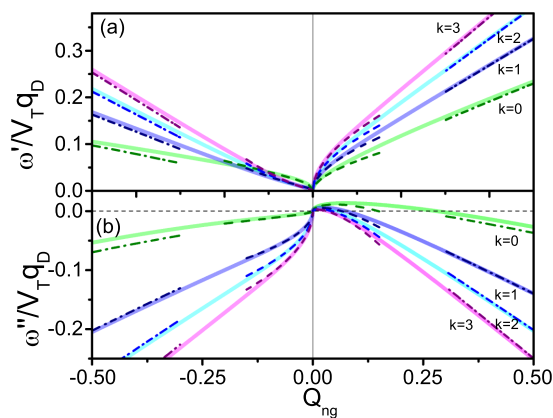


FIG. 8. The same as in Fig. 7 at $\mathcal{E}_{ng} = 0.15$. Dashed-dotted and dashed lines are the asymptotes calculated according to Eqs. (41) and (46) in the limit of $\mathcal{E} > 1/4\pi$, and $\gamma_q \gg 1$, respectively. The asymptote of the plasmonic mode for negative $q < 0$ (green dashed lines) is calculated according to Eqs. (43).

plasmonic modes and the higher-order thermal modes. This effect will be analyzed in detail in the Sec. V D.

The numerical calculations of the spectra of the thermal modes well reproduce the square-root dependence of $\omega'_k(q)$ and nonmonotonic behavior of the $\omega''_k(q)$ predicted by asymptotic expressions (46) at $q > 0$. For $q > 0$, the instability range also exists for the thermal modes, but it is more narrow than for the plasmonic mode. The instability range is farther narrowing for higher-order thermal modes. At $q < 0$, the thermal modes are overdamped oscillations with monotonic square-root wave-vector dependencies of ω' and ω'' at small Q_{ng} .

In the range of larger q ($Q_{ng} > 0.2$), the Landau damping effect prevails over the field effect. At this, the plasmonic mode, as well the thermal modes, has $\omega'' < 0$. For thermal modes, asymptotic expressions (46) are almost coincide with the numerical results. For plasmonic modes, these expressions also give satisfactory approximation.

At larger electric field $\mathcal{E}_{ng} = 0.15$, the effect of the electric field leads to essential increasing of both the instability range and the value of ω'' . As seen from Fig. 8, the plasmonic modes at $q > 0$ have lowest oscillation frequency among all modes and it is unstable in the wide range of $Q_{ng} = 0 \dots 0.25$. The instability range also essentially increases for the thermal modes. For example, the first thermal mode is unstable in the range of $Q_{ng} = 0 \dots 0.1$. The numerically obtained spectral characteristics of $\omega'_k(q)$ and $\omega''_k(q)$ are well described by Eqs. (46) in range of $Q_{ng} = 0 \dots 0.1$ where $\gamma_q > 1$. For negative q , the plasmonic mode is less sensitive to increase of the electric field and is described by the asymptotic expressions (43).

2. Gated 2DEG

As opposed to the case of the ungated 2DEG, for gated 2DEG the dimensionless parameter in Eqs. (24), which determines the roots $\xi_k(q)$ in the nonequilibrium case, is $\mathcal{E} = \mathcal{E}_g = Q_g \gamma_q$. It depends on the wave vector $\sim 1/q$ and becomes large at small q . To make the comparison easy, it is convenient to express \mathcal{E}_g through the independent on q parameter \mathcal{E}_{ng} characteristic for the ungated 2DEG: $\mathcal{E}_g = Q_g \mathcal{E}_{ng} / Q_{ng}$. Figure 9

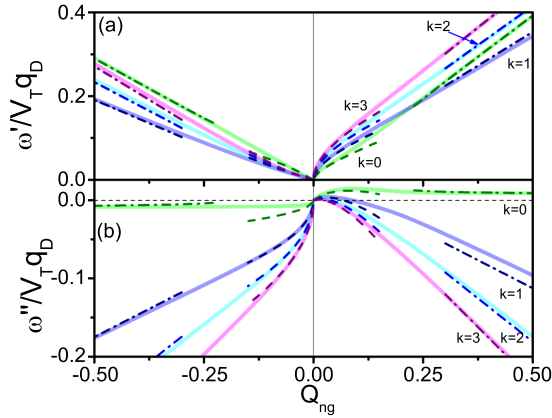


FIG. 9. The same as in Fig. 8 for the gated 2DEG at $\mathcal{E}_{ng} = 0.15$ and $Q_g = 0.05$. Dashed lines are the asymptotes calculated according to Eqs. (46) in the limit of $\mathcal{E} > 1/4\pi$, and $\gamma_q \gg 1$. The asymptotes of the plasmonic mode at larger values of $|Q_{ng}|$ (green dashed-dotted lines) are calculated according to Eqs. (44). The asymptotes of the thermal modes (colored dashed-dotted lines) are given by Eqs. (41).

demonstrates the plasmon spectra at a given \mathcal{E}_{ng} and relatively small parameter $Q_g = 0.05$ (the phase velocity of the gated plasmons V_p is much larger than the thermal velocity V_T).

We see that at small positive wave vectors $Q_{ng} < 0.1$ ($\gamma_q > 1$), the large effect of the electric field leads to the renormalization of $\omega'(q)$ and $\omega''(q)$ for both plasmonic and thermal modes. They acquired the square-root wave-vector dependencies of $\omega'(q)$ in the agreement with the asymptotic expressions (46). The behavior of the thermal modes is similar for the case of the ungated 2DEG. They possess a finite range of instability that decreases for the higher modes. The plasmonic modes are unstable in a wide range of Q_{ng} with almost constant increment and the linear dispersion of $\omega'(q)$. At negative q , the plasmonic mode is damped also with almost constant decrement. Such behavior of the plasmonic mode agrees with Eqs. (44).

D. Comparison of the excitation spectra of ungated and gated 2DEG at $\mathcal{E} \neq 0$

After general analysis of the collective excitations presented above, we consider the results obtained for a particular 2DEG. In Fig. 10 the numerical calculations of $\omega'_0(q)$ and $\omega''_0(q)$ are shown for the ungated and gated GaAs quantum wells. Two values of the electron concentration are assumed: $n_0 = 10^{11} \text{ cm}^{-2}$ and $3 \times 10^{11} \text{ cm}^{-2}$. The applied electric field is set $E_0 = 2 \text{ kV/cm}$. Other parameters are the same as in Sec. IV C. For these two concentrations we estimate the parameters as follows: $q_D/\kappa = 2 \times 10^6$ and $6 \times 10^6 \text{ cm}^{-1}$; $\mathcal{E}_{ng} = 0.11$ and 0.036 ; $Q_g = 0.43$ and 0.14 [see Eqs. (32)]. As seen in Fig. 10, both ungated and gated plasmonic modes demonstrate considerable nonreciprocal behavior.

For the positive wave vectors all the modes exhibit the instability. However, the instability range of the wave vectors and the increment ω'' strongly depend on parameters of 2DEG. The instability range for the ungated plasmonic mode at lower electron concentration is restricted by the condition $qd \sim 0.5$ ($d = 10 \text{ nm}$), while the increment can reach a value

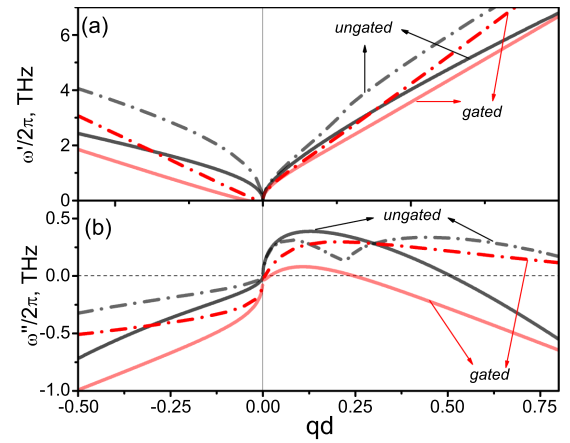


FIG. 10. Dependencies of $\omega'_0(q)$ (a) and $\omega''_0(q)$ (b) for the ungated (black lines) and gated (red lines) 2DEG in GaAs QW at two electron concentrations: $n_0 = 10^{11} \text{ cm}^{-2}$ (solid lines) and $3 \times 10^{11} \text{ cm}^{-2}$ (dashed-dotted lines). Other parameters are $E_0 = 2 \text{ kV/cm}$, $T_e = 100 \text{ K}$, $V_{dr} = 10^7 \text{ cm/s}$ ($V_{dr}/V_T = 0.5$), and $d = 10 \text{ nm}$.

$\approx 2.5 \text{ THz}$. At the same concentration, the gated plasmonic mode demonstrates the narrow instability range $qd < 0.2$, and smaller increment $\omega''_0 \approx 0.6 \text{ THz}$. The latter can be explained by larger Landau damping for the gated 2DEG.

At higher concentrations, the instability range for the ungated plasmonic mode is larger due to larger characteristic parameter q_D when the Landau damping decreases [see Eq. (43)]. The increment $\omega''(q)$ shows well-pronounced nonmonotonic behavior as a result of the interaction of the plasmonic and thermal modes. This effect will be illustrated in next subsection in details. An increase of the instability range at the larger electron concentration also occurs for the gated plasmonic mode, which is associated with decrease of the parameter Q_g [see Eqs. (32) and (45)]. At negative q decreasing of the electron concentrations always leads to an increase of the plasmonic mode damping.

E. Effect of the mode interaction

Now, we consider briefly interaction of the plasmonic and thermal modes. The effect of the interaction occurs at $q > 0$ in moderate electric fields ($\mathcal{E}_{ng} \lesssim 1/4\pi$). Figure 11 illustrates this effect for the ungated 2DEG. There, calculations of $\omega'_0(q)$ and $\omega''_0(q)$ are presented for $\mathcal{E}_{ng} = 0.03 \dots 0.07$. As seen, the well-pronounced interaction between plasmonic and thermal modes is observed for the fields $\mathcal{E}_{ng} = 0.03, 0.04$. The interaction modifies strongly the increment $\omega''(q)$ of the plasmonic mode [Fig. 11(b)], while the oscillation frequency $\omega'_0(q)$ is experiencing only small changes (see the inset in Fig. 11). With increasing of \mathcal{E}_{ng} the interaction effect becomes suppressed. At negative wave vectors ($q < 0$), the mode interaction effect is almost absent.

VI. INTERACTION OF ELECTROMAGNETIC WAVES WITH COLLECTIVE ELECTRON EXCITATIONS

The analyzed above spectra of the collective electron excitations determine interaction of 2DEG with electromagnetic waves of the relevant frequency range. In this section, we

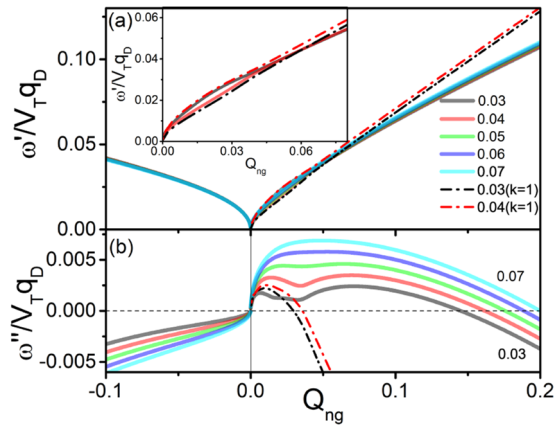


FIG. 11. Solid lines are dependencies of $\omega'(q)$ (a) and $\omega''(q)$ (b) numerically calculated for the plasmonic mode ($k = 0$) and at five values of $\mathcal{E}_{ng} = 0.03, 0.04, 0.05, 0.06, 0.07$. Black and red dashed-dotted lines correspond to the thermal mode with $k = 1$ at $\mathcal{E}_{ng} = 0.03$ and 0.04 , respectively. Inset magnifies the region of ω' with the mode interaction. The drift velocity $V_{dr}/V_T = 0.5$ is assumed to be same for all curves.

consider examples of such interaction. As indicated in the Introduction, a coupling of electromagnetic radiation and 2DEG can be provided by submicron or nanoscale lateral structuring of the sample. Below we consider grating-based plasmonic structure illustrated in Fig. 12(a). It consists of the AlGaAs/GaAs QW heterostructure with 2DEG and the periodic metallic grating. The grating is characterized by the period a_g and the width of metallic strips b_g .

The optical properties of the plasmonic structure, particularly absorption spectra, were determined by solving the Maxwell equations [16,59] with the high-frequency electron current calculated in the transport model of Sec. II. In this model, the high-frequency conductivity of the drifting electrons is frequency and wave-vector dependent [50]. For the calculations, we specified dependencies $V_{dr}(E_0)$ and $T_e(E_0)$ as shown in Fig. 12(b) (the case of the subthreshold Gunn electric fields). These dependencies were obtained by solving steady state the BTE within the electron temperature approach [55]. They are well correlated with early reported data [60,61]

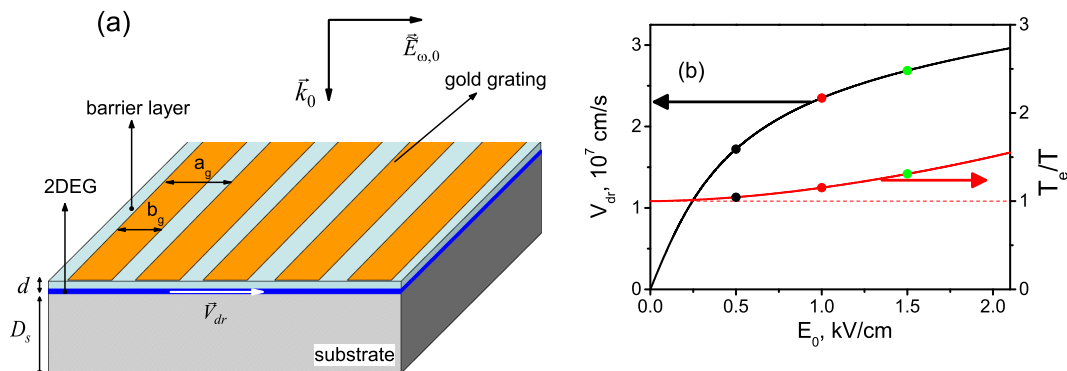


FIG. 12. (a) Sketch of grating-based plasmonic structure. (b) Dependencies of $V_{dr}(E_0)$ and $T_e(E_0)$ at $T = 77$ K calculated for 2DEG with low-field mobility of 8×10^4 cm²/Vs. The dots correspond to the electric fields for which the absorption spectra are shown in Fig. 13.

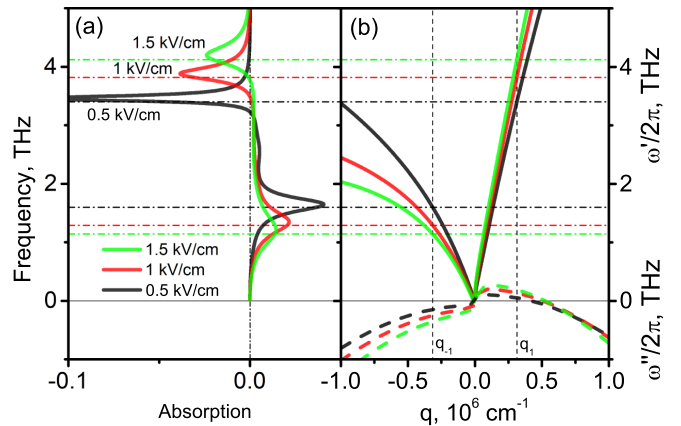


FIG. 13. (a) Absorption spectra of the plasmonic structure. (b) $\omega'_0(q)$ (solid lines) and $\omega''_0(q)$ (dashed lines), calculated numerically for $\kappa(|q|)$ given by Eq. (31) (b). The results presented for $n_0 = 3 \times 10^{11}$ cm⁻² and three values of the electric field. Horizontal lines denote the characteristic frequencies $\omega'_0(q_{\pm 1})$ and wave vectors $q_{\pm 1} = \pm 2\pi/a_g = \pm 0.31 \times 10^6$ cm⁻¹.

for 2DEG in high-quality GaAs QW with moderate electron concentrations of $1 - 5 \times 10^{11}$ cm⁻².

The absorption spectra were calculated for the plasmonic structure with narrow-slits grating with $a_g = 200$ nm, $b_g = 160$ nm, $d = 20$ nm, and $D_s = 2000$ nm. The results presented in Fig. 13(a) are obtained for different electric fields at a given electron concentration, while Fig. 14(a) shows the results for different electron concentrations and a given electric field. For easy interpretation of the results, the absorption spectra are compared with the dispersion of the plasmons of the gated 2DEG [see Figs. 13(b) and 14(b)]. Indeed, under narrow-slits grating the gated plasmon modes are predominantly excited.

As seen from Figs. 13 and 14, the absorption spectra demonstrate the resonant behavior. The frequencies of the resonances and signs corresponding to positive and negative absorption are well agreed with the parameters $\omega'_0(q_{\pm 1})$ and $\omega''_0(q_{\pm 1})$ of the plasmonic modes calculated at the wave vectors relevant to the grating period $q_{\pm 1} = \pm 2\pi/a_g$. Thus, excitations of different collective oscillations of 2DEG explain basic behavior of the absorption. The large drift velocities $V_{dr}(E_0)$ cause strongly nonreciprocal character of the plasmon

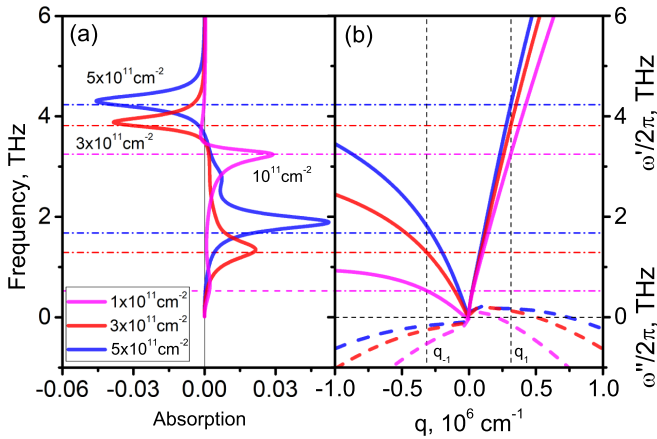


FIG. 14. The same as in Fig. 13 for three electron concentrations and $E_0 = 1$ kV/cm.

spectra and large splitting of the absorption spectra. Moreover, excitation of the plasmon waves with $q > 0$ causes the change of absorption of the incident radiation up to their amplification. The thermal modes are not observed in the absorption spectra because of their large damping at the wave vectors $q = q_{\pm 1}$.

Particularly, at $n_0 = 3 \times 10^{11} \text{ cm}^{-2}$, Fig. 13 shows “the frequency window” of the negative absorption (i.e., incident wave amplification) which is realized in the frequency range 3.5–5 THz at the electric field 0.5–1.5 kV/cm. The appearance of such a window corresponds to excitation of the unstable plasmon modes with $\omega'_0(q) > 0$, which propagate along the electron drift. In the low-frequency range ($\lesssim 2$ THz), the positive absorption corresponds to excitation of the damped plasmon modes propagating opposite to electron drift. Increase of the electric field leads to the blueshift (redshift) of the amplification (absorption) of the resonant lines with progressive increase of their broadening. This behavior relates to essential contribution of the Doppler-shift term and nontrivial impact of the electric field on the ballistic electron dynamics. The latter leads to a strong modification of $\omega'_0(q)$ for larger E_0 .

Figure 14(a) demonstrates considerable dependence of the absorption and amplification spectra on the electron concentrations: at $n_0 = 10^{11} \text{ cm}^{-2}$ the negative absorption effect is almost suppressed, while the effect is large for $n_0 = (3 \dots 5) \times 10^{11} \text{ cm}^{-2}$, which correlates with the plasmon parameters $\omega'(q)$ and $\omega''(q)$ presented in Fig. 14(b).

Finally, we estimate the criteria of the collisionless approach $\omega' \tau_{sc} \gg 1$ and $l_{sc} q \gg 1$, with τ_{sc} and $l_{sc} \approx V_T \tau_{sc}$ being the scattering time of and the mean-free path of the electrons, respectively. For the plasmonic structure with GaAs QW, we can use an effective scattering time of the hot electrons τ_{sc} that is found from the hot-electron mobility $\mu_{he} = dV_{dr}(E)/dE = e\tau_{sc}/m^*$. For the data presented in Fig. 10(b), we obtain $\mu_{he} \approx 10^4 \text{ cm}^2/\text{Vs}$ and $\tau_{sc} \approx 0.4 \text{ ps}$ at $E_0 = 1 \text{ kV/cm}$. At this field, the resonance and negative absorption occur at the frequency $\omega'/2\pi = 3.8 \text{ THz}$, which corresponds to the excitation of the unstable plasmon mode with the wave vector $q = 0.3 \times 10^6 \text{ cm}^{-1}$. Setting $V_T \approx 2 \times 10^7 \text{ cm/s}$ ($T = 100 \text{ K}$), we find

$l_{sc} \approx 100 \text{ nm}$. Then, we find $\omega' \tau_{sc} \approx 10$ and $q l_{sc} \approx 3$. Thus, the necessary criteria are reasonably satisfied.

VII. SUMMARY

We have developed theory of the collective electron oscillations of the 2DEG with attention to the case when a high electric field is applied. The effect of the stationary electric field has been taken into account on both the stationary and high-frequency electron transports. Two actual types of the structures with *ungated* and *gated* 2DEG have been considered (see illustration in Fig. 1). The analysis has been conducted basing on solutions of the Boltzmann-Vlasov equations in the collisionless approach, when the high-frequency electron transport is treated as ballistic. The system of equations, which determines the excitation spectra, has been presented in the form of Eqs. (24) applicable to both types of the structures: equilibrium and nonequilibrium conditions. Mapping the roots of these equations in Figs. 2, 5, and 6 facilitated understanding of the complexity of the excitation spectra. The numerical calculations of the excitation spectra have been supplemented by the asymptotic formulas.

We have found that the collective excitation spectra of 2DEG are of the multibranch character with the high-quality plasmonic modes and a set of the thermal modes. Under equilibrium, for the ungated 2DEG in the long-wavelength limit $Q_{ng} = \kappa|q|/q_D \ll 1$, the plasmonic modes have square-root wave-vector dependence of the oscillation frequency ω' and exponentially small damping ω'' . For the short wavelengths $Q_{ng} \sim 1$, the plasmonic modes acquire an essential damping, both $\omega'(q)$ and $\omega''(q)$ exhibit almost linear q dependencies. Oscillation frequency ω' and damping ω'' of the plasmonic modes are strongly influenced by the dielectric surroundings of the 2DEG.

For the gated 2DEG, in the limit of the thin barrier layer $qd \ll 1$ [see Fig. 1(b)], both $\omega'(q)$ and $\omega''(q)$ are the linear functions of q and their slopes are determined by the relationships between the phase velocity V_p [defined by Eq. (33)] and the thermal velocity V_T [see Eq. (21)]. At typical case $V_p \gg V_T$, the oscillation frequency almost coincides with the result of the hydrodynamic approximation: $\omega' = V_p|q|$. At this, the mode damping is exponentially small, $\omega'' \propto \exp(-V_p^2/V_T^2)$. The latter formula essentially differs from the usual Landau damping [43,44].

The thermal modes are the overdamped oscillations in the entire range of the wave vectors. Their appearance relates to the statistical treatment of the 2DEG. These modes are absent in the frameworks of the conventional hydrodynamic treatment of the 2DEG. The phase velocity and damping of these modes are determined by thermal velocity of the 2DEG, V_T . They are less sensitive to the dielectric surroundings.

Under nonequilibrium conditions, the high electric field can essentially modify the plasmon spectra of the 2DEG. The wave-vector dependencies of the oscillation frequency and damping/increment of the plasmonic and thermal modes manifest strong nonreciprocal behavior with respect to the direction of the applied field. The modes propagating opposite electron drift are always damped oscillations with $\omega'' < 0$. The increasing of the amplitudes of the applied electric field increases their damping. The modes propagating along

electron drift have the finite range of the wave vectors q , where they are unstable with $\omega'' > 0$. The instability range of q and amplitudes of the increment strongly depend on the type of the modes, dielectric surroundings, and amplitude of the applied electric field.

In the case of the ungated 2DEG, the spectral characteristics of the plasmonic modes depend on the following parameters: the dimensionless electric field $\mathcal{E}_{ng} = eE_0\kappa/k_B T_e q_D$ and the dimensionless wave vector $Q_{ng} = \kappa q/q_D$. For $Q_{ng}, \mathcal{E}_{ng} \ll 1$ and $2(Q_{ng} + \mathcal{E}_{ng}^2/Q_{ng}) \ll 1$, the oscillation frequencies ω' are weakly renormalized. However, instead of exponentially small damping, the plasmonic modes acquire $\omega''(q) > 0$ with the square-root wave-vector dependence and linear proportionality to E_0 , i.e., the plasmonic modes become unstable.

For a set of the thermal modes, the electric field also induces instability intervals at small positive q . However, these intervals are much narrower than for the plasmonic mode. In the range of the moderate applied electric field $\mathcal{E}_{ng} < 1/4\pi$, we found the effect of strong interaction of the plasmonic and thermal modes.

In the case of the gated 2DEG, in the limit of $|q|d \ll 1$, the spectral characteristics of the plasmonic mode are determined by the ratio of the thermal and phase velocities $Q_g = V_T^2/2V_p^2$ and dimensional electric field $\mathcal{E}_g = Q_g \gamma q$. For $Q_g, \mathcal{E}_g \ll 1$ and combination $2(Q_g + \mathcal{E}_g^2/Q_g) \ll 1$, the oscillation frequency ω' is weakly renormalized, however, the plasmonic modes possess a wide instability range with almost constant increment. The increment is proportional to E_0 . When $Q_g \sim 1$, the Landau damping mechanism suppresses the development of the plasmon instability.

It should be stressed that the studied electrically induced plasmon instability differs from the well-known Cherenkov mechanisms, which can be actual for systems with two mobile charged components (electrons + ions, electrons+polar optical phonons, two-stream plasma) or in the case of single-component plasma drifting under the grating, etc. Indeed, it is accepted that in uniform plasma with a single

mobile charged component (the electrons in the case of consideration) and with Maxwellian or shifted-Maxwellian distributions *there are no instabilities* [58,62]. The studied here instability is due to the impact of the electric field on high-frequency electron dynamics.

The effect of the plasmon instability can lead to the frequency windows of the negative absorption of THz radiation in the plasmonic structures with deeply submicron grating, as illustrated above for the example of the 2DEG in AlGaAs/GaAs. We estimated that the effect can be realized in the frequency range of 3–5 THz for moderate electron concentrations $(3\text{--}5) \times 10^{11} \text{ cm}^{-2}$ under the applied electric fields of 0.5–1.5 kV/cm. Although for these parameters the criteria necessary for application of the collisionless approximation are met, we suggest that more correct determination of characteristics of the negative absorption effect requires numerical solutions of the Boltzmann-Vlasov equations with electron relaxation processes included.

We suggest that presented results can be important for deeper understanding of the plasma physics of low-dimensional structures and useful for development of electrically pumping THz optoelectronic devices.

ACKNOWLEDGMENTS

This work was supported by the Ministry of Education and Science of Ukraine (Project No. M/24-2018), by the German Federal Ministry of Education and Research (BMBF Project No. 01DK17028), and by the Research Council of Lithuania (Lietuvos mokslo taryba) under the “KOTERAPLAZA” Project (Grant No. DOTSUT-247) funded by the European Regional Development Fund according to the supported activity “Research Projects Implemented by World-class Researcher Groups” under Measure No. 01.2.2-LMT-K-718-0047. The authors are sincerely grateful to Dr. I. Kašalynas for fruitful discussions of the various aspects of this work.

-
- [1] A. V. Chaplik, *Surf. Sci. Rep.* **5**, 289 (1985).
 [2] V. V. Popov, *J. Infrared Milli Terahz Waves* **32**, 1178 (2011).
 [3] A. A. Zabolotnykh and V. A. Volkov, *Phys. Rev B* **99**, 165304 (2019).
 [4] T. Otsuji, V. Popov, and V. Ryzhii, *J. Phys. D: Appl. Phys.* **47**, 094006 (2014).
 [5] S. M. Kukhtaruk and V. A. Kochelap, *Phys. Rev. B* **92**, 041409(R) (2015).
 [6] A. Nemilentsau, T. Low, and G. Hanson, *Phys. Rev. Lett.* **116**, 066804 (2016).
 [7] T. Otsuji and M. Shur, *IEEE Microwave Mag.* **15**, 43 (2014).
 [8] S. J. Allen, Jr., D. C. Tsui, and R. A. Logan, *Phys. Rev. Lett.* **38**, 980 (1977).
 [9] M. Bialek, M. Czapkiewicz, J. Wrybel, V. Umansky, and J. Lusakowski, *Appl. Phys. Lett.* **104**, 263514 (2014).
 [10] A. Muravjov, D. Veksler, V. Popov, O. Polischuk, N. Pala, X. Hu, R. Gaska, H. Saxena, R. Peale, and M. Shur, *Appl. Phys. Lett.* **96**, 042105 (2010).
 [11] V. A. Shalygin, M. D. Moldavskaya, M. Ya. Vinnichenko, K. V. Maremyanin, A. A. Artemyev, V. Yu. Panevin, L. E. Vorobjev, D. A. Firsov, V. V. Korotyeyev, A. V. Sakharov, E. E. Zavarin, D. S. Arteev, W. V. Lundin, A. F. Tsatsulnikov, S. Suihkonen, and C. Kauppinen, *J. Appl. Phys.* **126**, 183104 (2019).
 [12] H. Yan, X. Li, Bh. Chandra, G. Tulevski, Y. Wu, M. Freitag, W. Zhu, Ph. Avouris, and F. Xia, *Nat. Nanotechnol.* **7**, 330 (2012).
 [13] B. Yan, J. Fang, Sh. Qin, Y. Liu, Y. Zhou, R. Li, and X.-A. Zhang, *Appl. Phys. Lett.* **107**, 191905 (2015).
 [14] D. S. Jessop, S. J. Kindness, L. Xiao, P. Braeuninger-Weimer, H. Lin, Y. Ren, C. X. Ren, S. Hofmann, J. A. Zeitler, H. E. Beere, D. A. Ritchie, and R. Degl’Innocenti, *Appl. Phys. Lett.* **108**, 171101 (2016).
 [15] A. S. Bhatti, D. Richards, H. P. Hughes, and D. A. Ritchie, *Phys. Rev. B* **53**, 11016 (1996).
 [16] Yu. M. Lyaschuk and V. V. Korotyeyev, *Ukr. J. Phys.* **62**, 889 (2017).

- [17] T. Wenger, G. Viola, J. Kinaret, M. Fogelström and Ph. Tassin, *Phys. Rev. B* **97**, 085419 (2018).
- [18] D. Svintsov, *Phys. Rev. B* **100**, 195428 (2019).
- [19] S. A. Boubanga-Tombet, D. Yadav, A. Satou, W. Knap, V. V. Popov, and T. Otsuji, *Proc. SPIE* **11348**, 113480P (2020).
- [20] G. R. Aizin, V. V. Popov, and O. V. Polischuk, *Appl. Phys. Lett.* **89**, 143512 (2006).
- [21] V. V. Popov, D. V. Fateev, T. Otsuji, Y. M. Meziani, D. Coquillat, and W. Knap, *Appl. Phys. Lett.* **99**, 243504 (2011).
- [22] K. Nogajewski, J. Lusakowski, W. Knap, V. V. Popov, F. Teppe, S. L. Romyantsev, and M. S. Shur, *Appl. Phys. Lett.* **99**, 213501 (2011).
- [23] D. M. Yermolayev, K. M. Maremyanin, D. V. Fateev, S. V. Morozov, N. A. Maleev, V. E. Zemlyakov, V. I. Gavrilenko, S. Yu. Shapoval, F. F. Sizov, and V. V. Popov, *Solid-State Electron.* **86**, 64 (2013).
- [24] D. A. Bandurin, D. Svintsov, I. Gayduchenko, Sh. G. Xu, A. Principi, M. Moskotin, I. Tretyakov, D. Yagodkin, S. Zhukov, T. Taniguchi, K. Watanabe, I. V. Grigorieva, M. Polini, G. N. Goltsman, A. K. Geim, and G. Fedorov, *Nat. Commun.* **9**, 5392 (2018).
- [25] H. Qin, Y. Yu, X. Li, J. Sun, and Y. Huang, *Int. J. Terahertz Sci. Technol.* **9**, 71 (2016).
- [26] V. Jakštas, I. Grigelionis, V. Janonis, G. Valušis, I. Kašalynas, G. Seniutinas, S. Juodkazis, P. Prystawko, and M. Leszczynski, *Appl. Phys. Lett.* **110**, 202101 (2017).
- [27] R. A. Hopfel, E. Vass, and E. Gornik, *Phys. Rev. Lett.* **49**, 1667 (1982).
- [28] M. V. Krasheninnikov and A. V. Chaplik, *Zh. Eksp. Teor. Fiz.* **88**, 129 (1985) [*JETP* **61**, 75 (1985)].
- [29] M. Dyakonov and M. Shur, *Phys. Rev. Lett.* **71**, 2465 (1993).
- [30] S. Rudin and G. Rupper, *Jpn. J. Appl. Phys.* **52**, 08JN25 (2013).
- [31] M. V. Cherenisin and G. G. Samsonidze, *Solid-State Electron.* **52**, 338 (2008).
- [32] Z. S. Gribnikov, N. Z. Vagidov, V. V. Mitin, and G. I. Haddad, *J. Appl. Phys.* **93**, 5435 (2003).
- [33] V. V. Korotyevev, V. A. Kochelap, A. A. Klimov, G. Sabatini, H. Marinchio, C. Palermo, and L. Varani, *J. Nanoelectron. Optoelectron.* **6**, 169 (2011).
- [34] V. Ryzhii, A. Satou, M. Ryzhii, T. Otsuji, and M. S. Shur, *J. Phys.: Condens. Matter* **20**, 384207 (2008); This paper proposed a possible mechanism of the THz emission observed in the experiments with grating-gated FET [T. Otsuji *et al.*, *Appl. Phys. Lett.* **89**, 263502 (2006); Y. M. Meziani *et al.*, *ibid.* **90**, 061105 (2007)].
- [35] V. I. Ryzhii, N. A. Banov, and V. A. Fedirko, *Fiz. Tekh. Poluprovodn.* **8**, 769 (1984) [*Sov. Phys.–Semicond.* **18**, 769 (1984)].
- [36] S. A. Mikhailov, *Phys. Rev. B* **58**, 1517 (1998); *Recent Res. Devel. Appl. Phys.* **2**, 65 (1999).
- [37] A. S. Petrov, D. Svintsov, V. Ryzhii, and M. S. Shur, *Phys. Rev. B* **95**, 045405 (2017).
- [38] S. M. Komirenko, K. W. Kim, V. A. Kochelap, I. Fedorov, and M. A. Stroschio, *Appl. Phys. Lett.* **77**, 4178 (2000); *Phys. Rev. B* **63**, 165308 (2001).
- [39] W. Liang, K. T. Tsen, O. F. Sankey, S. M. Komirenko, K. W. Kim, V. A. Kochelap, MengChyi Wu, Chong-Long Ho, Wen-Jeng Ho, and H. Morkoc, *Appl. Phys. Lett.* **82**, 1968 (2003); K. T. Tsen, J. Kiang, D. K. Ferry, V. A. Kochelap, S. M. Komirenko, K. W. Kim, and H. Morkoc, *J. Phys.: Condens. Matter* **18**, 7961 (2006).
- [40] O. Sydoruk, E. Shamonina, V. Kalinin, and L. Solymar, *Phys. Plasmas* **17**, 102103 (2010).
- [41] M. Woerner, C. Somma, K. Reimann, T. Elsaesser, P. Q. Liu, Y. Yang, J. L. Reno, and I. Brener, *Phys. Rev. Lett.* **122**, 107402 (2019).
- [42] V. A. Kochelap, V. V. Korotyevev, Yu. M. Lyashchuk and K. W. Kim, *J. Appl. Phys.* **126**, 085708 (2019).
- [43] L. D. Landau, *Zh. Eksp. Teor. Fiz.* **16**, 574 (1946) [*Acad. Sci. USSR. J. Phys.* **10**, 25 (1946)]; see also, *Collected Papers of L.D. Landau*, edited by D. TerHaar (Pergamon, 1965), pp. 445–460.
- [44] B. B. Kadomtsev, *Sov. Phys.–Usp.* **11**, 328 (1968).
- [45] H. Totsuji, *J. Phys. Soc. Jpn.* **40**, 857 (1976).
- [46] A. I. Akhiezer and A. G. Sitenko, *Zh. Eksp. Teor. Fiz.* **30**, 216 (1956) [*JETP* **3**, 140 (1956)].
- [47] Ben Yu-Kuang Hu and J. W. Wilkins, *Phys. Rev. B* **39**, 8464 (1989).
- [48] Ben Yu-Kuang Hu and J. W. Wilkins, *Phys. Rev. B* **43**, 14009 (1991).
- [49] S. A. Mikhailov, N. A. Savostianova, and A. S. Moskalenko, *Phys. Rev. B* **94**, 035439 (2016).
- [50] V. V. Korotyevev, V. A. Kochelap, S. Danylyuk, and L. Varani, *Appl. Phys. Lett.* **113**, 041102 (2018).
- [51] Y. Koseki, V. Ryzhii, T. Otsuji, V. V. Popov, and A. Satou, *Phys. Rev. B* **93**, 245408 (2016).
- [52] The similar picture of the plasmon spectra was discussed for nonequilibrium 2DEG with strongly anisotropic distribution function in V. V. Korotyevev, V. A. Kochelap, and L. Varani, *J. Appl. Phys.* **112**, 083721 (2012).
- [53] G. P. M. Poppe and C. M. J. Wijers, *ACM Trans. Math. Software* **16**, 38 (1990).
- [54] S. M. Komirenko, K. W. Kim, V. A. Kochelap, V. V. Koroteev, and M. A. Stroschio, *Phys. Rev. B* **68**, 155308 (2003).
- [55] V. V. Korotyevev, *Semicond. Phys., Quantum Electron. Optoelectron.* **18**, 1 (2015).
- [56] E. A. Jackson, *Phys. Fluids* **3**, 786 (1960).
- [57] Hua-Sheng Xie, *Phys. Plasmas* **20**, 092125 (2013).
- [58] O. Penrose, *Phys. Fluids* **3**, 258 (1960).
- [59] O. R. Matov, O. V. Polischuk, and V. V. Popov, *Int. J. Infrared Millimeter Waves* **14**, 1455 (1993).
- [60] W. Ted Masselink, *Semicond. Sci. Technol.* **4**, 503 (1989).
- [61] M. Moško and A. Mošková, *Phys. Rev. B* **44**, 10794 (1991).
- [62] N. A. Krall and A. W. Trivelpiece, *Principles of Plasma Physics* (McGraw-Hill, New York 1973).